

MacKenzie, L.E., Choudhary, T.R., McNaught, A.I., and Harvey, A.R. (2016) In vivo oximetry of human bulbar conjunctival and episcleral microvasculature using snapshot multispectral imaging. *Experimental Eye Research*, 149, pp. 48-58. (doi:[10.1016/j.exer.2016.06.008](https://doi.org/10.1016/j.exer.2016.06.008))

This is the author's final accepted version.

There may be differences between this version and the published version. You are advised to consult the publisher's version if you wish to cite from it.

<http://eprints.gla.ac.uk/136058/>

Deposited on: 02 February 2017

# ***In vivo* oximetry of human bulbar conjunctival and episcleral microvasculature using snapshot multispectral imaging**

**L.E. MacKenzie,<sup>1</sup> T.R. Choudhary,<sup>2,3</sup> A.I. McNaught,<sup>4,5</sup> and A.R. Harvey.<sup>1</sup>**

1. School of Physics and Astronomy, University of Glasgow, Glasgow, United Kingdom.

2. Institute of Biological Chemistry, Biophysics and Bioengineering, Heriot-Watt University, Edinburgh, United Kingdom.

3. EPSRC IRC "Hub" in Optical Molecular Sensing & Imaging, MRC Centre for Inflammation Research, Queen's Medical Research Institute, University of Edinburgh, Edinburgh, UK

4. Department of Ophthalmology, Cheltenham General Hospital, Gloucestershire Hospitals NHS Foundation Trust, Gloucestershire, United Kingdom.

5. Department of Health Professions, Plymouth University, Plymouth, United Kingdom.

**Correspondence:** Andrew Harvey, School of Physics & Astronomy, Kelvin Building, University of Glasgow, Glasgow, G12 8QQ, United Kingdom;

[Andy.Harvey@glasgow.ac.uk](mailto:Andy.Harvey@glasgow.ac.uk)

## Abstract

Multispectral imaging (MSI) is now well established for non-invasive oximetry of retinal blood vessels, contributing to the understanding of a variety of conditions affecting the retinal circulation, including glaucoma, diabetes, vessel occlusion, and auto-regulation. We report the application of a unique snapshot MSI technique to enable the first oximetric imaging of the blood vessels of the anterior segment, i.e. the episcleral and bulbar conjunctival microvasculature. As well as providing a new capability of oximetry of the scleral vasculature, this technique represents ocular oximetry that is complimentary or alternative to retinal oximetry. We report the oxygen dynamics of these microvascular beds and assess how acute mild hypoxia effects the blood oxygen saturation ( $SO_2$ ) of bulbar conjunctival and episcleral microvasculature.

A retinal-fundus camera fitted with a custom Image-Replicating Imaging Spectrometer enabled oximetric imaging of bulbar conjunctival and episcleral microvasculature in ten healthy human subjects at normoxia (21% Fraction of Inspired Oxygen [ $FiO_2$ ]) and acute mild-hypoxia conditions (15%  $FiO_2$ ). Eyelid closure was used to block oxygen diffusion between ambient air and the sclera surface. Four of the ten subjects – those that presented suitable vasculature for direct comparison between bulbar conjunctival and episcleral vessels - were imaged for 30 seconds following eyelid opening. Vessel diameter and Optical Density Ratio (ODR: a direct proxy for oxygen saturation) of vessels was computed automatically. Oximetry capability was validated using a simple phantom for the scleral vasculature,

Average episcleral diameter increased from  $78.9 \pm 8.7\mu m$  (mean  $\pm$  standard deviation) at normoxia to  $97.6 \pm 14.3\mu m$  at hypoxia ( $p = 0.02$ ). Diameters of bulbar conjunctival vessels showed no significant change from  $80.1 \pm 7.6\mu m$  at normoxia to

80.6 ± 7.0µm at hypoxia (p= 0.89). Acute mild hypoxia resulted in a decrease in SO<sub>2</sub> (i.e. an increase in ODR) from normoxia levels in both bulbar conjunctival (p <0.001) and episcleral vessels (p= 0.03).

Hypoxic bulbar conjunctival vasculature rapidly re-oxygenated in an exponential manner, reaching normoxia baseline levels, with an average ½ time to full reoxygenation of 3.4 ±1.4 seconds. This reoxygenation occurs because the bulbar conjunctival vessels are in direct contact with ambient air. This is the first study to characterise and also to image the oxygen dynamics of bulbar conjunctival and episcleral microvasculature, and to directly observe the rapid reoxygenation of hypoxic bulbar conjunctival vessels when exposed to air.

Oxygen diffusion into the bulbar conjunctiva must be taken into account to provide meaningful oximetry because bulbar conjunctival vessels will be highly oxygenated (close to 100% SO<sub>2</sub>) when exposed to ambient air.

Oximetry of bulbar conjunctival vessels could potentially provide insight into conditions where oxygen dynamics of the microvasculature are not fully understood, such as diabetes, sickle-cell diseases, and dry-eye syndrome. Further, *in vivo* oximetry of individual capillaries and groups of flowing red blood cells could be achieved with a high magnification slit lamp adapted for MSI.

**Keywords:** multispectral imaging, oximetry, hypoxia, bulbar conjunctiva, episclera, oxygen saturation, microvasculature, oxygen diffusion,

## 1. Introduction

Multispectral imaging (MSI) is well established for non-contact oximetry of blood vessels (D J Mordant et al., 2011a; David J Mordant et al., 2011b) which has enhanced the understanding of a variety of retinal conditions, such as diabetes (Hammer et al., 2009; Hardarson and Stefánsson, 2012; Isenberg et al., 1986), glaucoma (Boeckaert et al., 2012; Mordant et al., 2014; Olafsdottir et al., 2011), and vessel occlusion (Eliasdottir et al., 2014), as well as auto-regulation response to flicker stimulation (Hammer et al., 2011) and acute mild hypoxia (Choudhary et al., 2013). However, oximetry of capillaries in the retina is beyond the technical capabilities of MSI-enabled retinal fundus cameras. The anterior segment provides two alternative ocular microvascular beds that are easily accessible for multispectral imaging and which could be used to probe ocular blood oxygen saturation and potentially provide new physiologically-relevant information; the bulbar conjunctival and episcleral microvascular beds. This is the first study to use MSI to non-invasively measure the oxygen saturation of bulbar conjunctival and episcleral microvasculature with high spatial and temporal resolution, revealing rapid oxygen diffusion from ambient air into bulbar conjunctival vessels.

The episcleral microvasculature is located within the scleral tissue, with few episcleral vessels visible near the scleral surface. In contrast, the bulbar conjunctival microvasculature is semi-mobile above the sclera, and presents many arterioles, venules, and capillaries for imaging (Meighan, 1956). Groups of individual red blood cells can be observed to flow in bulbar conjunctival capillaries if imaged with high magnification (Jiang et al., 2014). The bulbar conjunctiva may be unique in that it is the only microvascular bed in the human body which is directly exposed to ambient air. Figure 1a shows generalised vessel positions with respect to the sclera. Figure 1b shows a representative image of bulbar conjunctival and episcleral vasculature in

a single subject. However, despite potential for new oximetry information and ease of imaging, no MSI oximetry studies of either the bulbar conjunctival or episcleral microvasculature have been published to date.

MSI oximetry is based on the  $\text{SO}_2$ -dependent optical absorption spectra of haemoglobin. Changes in  $\text{SO}_2$  can be calculated by imaging blood vessels at two wavelengths: one wavelength where optical absorption is sensitive to variations in  $\text{SO}_2$ , and at another wavelength which is insensitive to  $\text{SO}_2$  variations (i.e. isobestic). From images of vessels, the optical density (OD) of vessels at each wavelength can be calculated, allowing the calculation of optical density ratio (ODR); ODR is directly proportional to  $\text{SO}_2$ . In vessels where  $\text{SO}_2$  is known, ODR can then be empirically calibrated to  $\text{SO}_2$  by assuming local arterial  $\text{SO}_2$  is equal to the  $\text{SO}_2$  of systemic arterial  $\text{SO}_2$  as measured by pulse oximetry (Beach et al., 1999), or by using reference values from previous studies. (Hardarson et al., 2006).

To the best of our knowledge there are no reported MSI oximetry studies of the bulbar conjunctival or episcleral microvasculature. Instead, insights into the oxygen dynamics of microvasculature have generally been indirectly inferred from vessel-diameter or blood-flow measurements (Jiang et al., 2013; Shahidi et al., 2010; Wanek et al., 2013), however these parameters may be affected by factors other than changes in  $\text{SO}_2$ , such as conjunctival or episcleral inflammation. Direct measurement of the partial pressure of oxygen ( $\text{pO}_2$ ) of the palpebral conjunctival microvasculature has been achieved with Clark-type electrodes (Chapman et al., 1986; Iguchi et al., 2005; Isenberg et al., 2002; Kwan and Fatt, 1971; Mader et al., 1987), however these electrodes have insufficient spatial discrimination for localisation of oximetry to blood vessels and crucially, block oxygen diffusion between ambient air and blood vessels under study.

129

130 In this study, we report the use of a retinal fundus camera modified for Snapshot  
131 Multispectral Imaging (SMSI) to non-invasively quantify the oxygen dynamics of both  
132 bulbar conjunctival and episcleral microvasculature in ten healthy human subjects.  
133 The high temporal resolution of the SMSI system (10ms exposure, 1Hz image  
134 acquisition rate) enables observation of fast biological processes (Fernandez  
135 Ramos et al., 2014). We observe rapid oxygen diffusion from ambient air into bulbar  
136 conjunctival vessels due to the unique location of the bulbar conjunctiva (i.e. directly  
137 in contact with ambient air); such observations are not possible with time-sequential  
138 MSI or Clarke-type electrodes because these techniques lack sufficient temporal and  
139 spatial resolution respectively.

140

## 141 **2. Material and methods**

### 142 **2.1. Subject recruitment**

143 This study was approved by the Ethics Committee of the University of Glasgow,  
144 College of Medical, Veterinary and Life Sciences. All volunteers provided written  
145 informed consent before participation and all procedures were performed in  
146 accordance with the tenets of the Declaration of Helsinki. Ten healthy volunteers  
147 (age  $25 \pm 2$  years, six males and four female) were recruited. Subjects reported no  
148 history of ocular, respiratory, or vascular disease. Volunteers that regularly wore  
149 contact lenses or who were suffering from allergic conjunctivitis were excluded  
150 because this may induce fluctuating bulbar conjunctival vasodilatation (Gartner,  
151 1944; Cheung et al., 2012; Jiang et al., 2014) .

152

### 153 **2.2. Imaging system**

154 The imaging system consisted of a commercial retinal fundus camera (Topcon  
155 TR50-DX; Topcon, Itabashi, Tokyo, Japan), fitted with an Image Replicating Imaging

Spectrometer (IRIS) and a cooled sCMOS camera (Zyla 5.5; Andor, Belfast, United Kingdom). IRIS is discussed in detail elsewhere ( Harvey et al., 2005; Alabboud et al., 2007; Gorman et al., 2010; Fernandez Ramos et al., 2014); but in brief, IRIS simultaneously spectrally de-multiplexes a white-light image into eight distinct narrowband spectral images onto a single detector without rejection of light. Orthogonal-polarization imaging was used to minimise specular reflections from the sclera and blood vessels (van Zijderveld et al., 2014). Fundus-camera flash and image acquisition were synchronized using a custom graphical user interface written in LabVIEW, and images were saved in uncompressed Tiff format. Image acquisition was limited to 1Hz by the fundus camera flash refresh rate with an exposure time of 10ms. This imaging set-up and a representative multispectral IRIS image of the sclera are shown in Figure 2.

The curved scleral surface presents a challenge for imaging because it causes the position of blood vessels to vary with respect to the imaging plane of the fundus camera, potentially up to ~12mm from the anterior segment to the extreme lateral side of the sclera. To insure sharp focus over an extended scleral region, the 'small aperture' setting of the fundus camera was selected. This resulted in an estimated depth-of-field (DOF) of ~10mm; DOF was estimated by imaging a USAF test chart (USAF 1951 Chart; Applied Image Group-Imaging, Rochester, New York, USA) as it was moved through prime-focus on a linear-translation stage. A 35-degree field-of-view was selected to provide a field of view at the object plane of approximately 85 x 45mm. This combination of settings enabled the imaging of bulbar conjunctival and episcleral vessels over an extended scleral region with an optimal, sharp focus.

### **2.3. Scleral phantom**



For assessment of the validity of our oximetry technique, a simple sclera-mimicking phantom was manufactured (see Figure 3). Similar phantoms have previously been used to validate retinal oximetry (David J Mordant et al., 2011). The phantom consisted of a transparent Fluorinated Ethylene Propylene (FEP) capillary of 100µm inner diameter (Zuess inc., Belfast, Northern Ireland), placed in contact with optical-grade *Spectralon* (Spectralon® Diffusion Material; Labsphere inc, North Suttan, New Hampshire, USA); *Spectralon* has similar spectral reflectance characteristics to the sclera (Bashkatov et al., 2010; Labsphere Inc.). To simulate *in vivo* blood circulation, *ex vivo* whole horse blood (40% hematocrit) (E&O labs, Bonnybridge, Scotland, United Kingdom) was flowed through the FEP capillary under feed from a syringe pump (KDS260, Linton Instrumentation, UK). SO<sub>2</sub> of the blood was reduced by adding measured quantities of Sodium Dithionite (EMD Millipore, Fisher Scientific, Loughborough, UK) to 5ml samples of blood according to the procedure described in Briely-Sabo and Bjornerud (Briley-Saebo and Bjornerud, 2000). SO<sub>2</sub> blood samples was measured prior to imaging using an optical blood gas analyser (GEM OPL, Instrumentation Laboratory, Bedford, Massachusetts, USA). A total of eight SO<sub>2</sub> samples ranging between 5% and 100% SO<sub>2</sub> were imaged in the FEP capillary.

#### **2.4.1. Experimental procedure for *in-vivo* imaging**

Subjects positioned their head in the standard fundus-camera chin-rest; head-straps were used to restrain the subject and minimise any motion. The fundus camera objective lens was positioned approximately five centimetres from the subject's sclera. In this configuration, the fundus camera illumination formed a circle approximately four centimetres in diameter. Subject gaze was controlled by the subject fixating on the fundus camera external fixation target (a movable red LED). For each subject, the scale of images was determined by imaging a millimeter scale placed in front of the sclera at prime focus. All subsequent images were acquired at

this focal position. This enabled a calibration of the size of each pixel on the detector to the real size of an image; on average, one pixel corresponded to ~13.5 microns. From this, the measured vessel diameter in pixels was calibrated to diameter in microns.

Scleral regions of each subject were selected for imaging so as to maximise the number of bulbar conjunctival vessels meeting the inclusion criteria (see Section 2.6.1). Bulbar conjunctival and episcleral vasculature was distinguished by moving the gaze of a subject; this moved the position of the bulbar conjunctiva above the sclera, altering the relative position of bulbar conjunctival and episcleral vessels. However it was not possible to classify individual vessels as arterioles and venules because of the diverse morphology of bulbar conjunctival vasculature and the limited number of episcleral vessels available for imaging (see Section 4.4). Scleral regions were chosen for imaging so as to maximise the number of bulbar conjunctival vessels meeting inclusion criteria whilst including some episcleral vessels for analysis (see Section 2.6.1). Once selected, the same blood vessels in a single scleral region of a single eye for each subject were consistently imaged and analysed throughout the experiment.

Throughout the imaging protocol, the scleral region exposed to air was kept constant by the subject constantly gazing at the stationary fixation target and peripheral arterial  $SO_2$  was recorded throughout the experiment using a fingertip pulse oximeter (AUTOCORR; Smiths Medical ASD Inc., Rockland, MA, USA) interfaced to a computer using a custom LabVIEW interface.

#### **2.4.2. Repeatability**

To assess repeatability of ODR measurement, eight consecutive images of the same scleral region were acquired in a period of approximately ten seconds for each subject. Gaze fixation was maintained for 2.5 minutes with their eyelid open prior to imaging to expose the target vasculature to ambient air.

#### **2.4.3. Effect of eyelid closure**

Eyelid closure was used to control oxygen diffusion. Eyelid closure places a tissue barrier between the scleral surface and the ambient air, drastically decreasing the rate of any oxygen diffusion from ambient air to this scleral surface. To assess if eye closure affects the ODR of vessels, subjects were imaged before and after a period of eyelid closure. As before, subjects continually gazed at the fixation target for 2.5 minutes to expose the target vasculature to ambient air prior to imaging; subjects then closed their eyelids for a further 2.5 minutes. After 2.5 minutes of eyelid closure subjects opened their eyelid and synchronised imaging occurred

#### **2.5.4. Acute mild hypoxia**

To assess the effects of acute mild hypoxia on ODR, subjects were imaged at normoxia and acute mild-hypoxia. For normoxia measurement, subjects inhaled room air (21% FiO<sub>2</sub>) for 2.5 minutes whilst fixating on the red LED fixation target, after which they were imaged. To induce acute mild hypoxia, subjects closed their eyelids and breathed a hypoxic air mixture (15% 2.5 minutes of inhalation of hypoxic air mixture (15% FiO<sub>2</sub>) supplied via a hypoxic-air generator (Everest Summit II Hypoxic Generator; Hypoxico, Inc., New York, NY, USA) (Spurling et al., 2011). The hypoxic-air generator was calibrated before use and the air supply was monitored with an in-line oxygen analyzer (AD300 oxygen analyser; Teledyne Analytical Instruments, City of Industry, California, USA). Hypoxic air generators have been

previously used for a study into retinal response to acute mild hypoxia (Choudhary et al., 2013).

After 2.5 minutes of hypoxic-air inhalation, subjects opened their eyelids and synchronised imaging occurred. Synchronisation of imaging with events, such as eyelid opening, was accomplished with a five-second oral countdown and with an accuracy of  $\pm 1$  seconds. Subjects were then returned to normoxia by breathing room air. This process was repeated in the following sequence: normoxia 1, hypoxia 1, normoxia 2, hypoxia 2, normoxia 3; this sequence provides a robust time-sequential modulation in  $SO_2$  and associated ODR change that is highly distinct from normal physiological variations.

#### **2.5.5. Exposure of hypoxic vasculature to ambient air**

A sub-group of four subjects (3 male, 1 female) were selected for further study. These subjects presented bulbar conjunctival and episcleral vessels suitable for analysis within single scleral region, allowing concurrent imaging - and thus comparison of oxygen dynamics - between bulbar conjunctival and episcleral vessels. Hypoxia was induced as described in section 2.5.3. However, when subjects opened their eyelids, a synchronised 1Hz frame-rate imaging sequence was subsequently recorded for the 30 seconds, enabling observation of any rapid diffusion processes. This was repeated twice per subject.

### **2.6. Image analysis**

#### **2.6.1 Vessel section inclusion criteria**

The following inclusion criteria were applied to ensure that only appropriate vessel sections were selected for analysis: (1) vessel sections had to be greater than 5 pixels ( $\sim 65\mu m$ ) in diameter with no other vessel sections within 12 pixels either side;

the presence of small vessels was accepted due to the high density of small bulbar conjunctival vessels; (2) vessel sections had to be at least 30 pixels long (~390µm); (3) vessels close to vessel intersections, regions of scleral glare, specular reflections, or images with poor focus were excluded; (4) episcleral vessels had to be of high apparent contrast with respect to the scleral tissue and not show a significant decrease in contrast along the analysed vessel section length (i.e. not appear to go deeper in the sclera tissue); (5) vessel sections had to meet all these inclusion criteria for all images in each section of the study.

### **2.6.2. Vessel tracking**

Image processing was implemented *post hoc* using custom algorithms implemented in MATLAB. Raw IRIS images were cropped and co-registered to create a multispectral data cube. Vessels were tracked semi-automatically using manually identified control points. Repeated semi-automatic tracking demonstrated negligible variation in ODR (a standard deviation of <0.5% in 10 repeated measurements). Fully automatic tracking was not implemented because inter-image registration of bulbar conjunctival vessels is affected by the relative motion of bulbar conjunctival and episcleral vasculature (Crihalmeanu and Ross, 2012).

### **2.6.3. Oximetric analysis and vessel diameter measurement**

Our oximetric analysis is based on two-wavelength oximetry developed by Beach et al (Beach et al., 1999). For two-wavelength oximetry, the optical-density (OD) of blood vessels at two spectral wavebands is calculated: one waveband where optical absorption is insensitive to changes in SO<sub>2</sub> (isobestic) and one waveband where optical absorption is sensitive to changes in SO<sub>2</sub> (contrast). The 570nm IRIS waveband was utilised as the isobestic reference and the 560nm waveband was used as the oxygen sensitive waveband (Prahl, 1999). Each waveband has a full

spectral-width of approximately 7nm (Fernandez Ramos et al., 2014). Simple modelling based upon the Beer-Lambert law of optical absorption shows that the OD of blood vessels of ~60-100µm at 560nm and 570nm wavebands is expected to be between 0.15 and 1; near-optimal for oximetry (van Assendelft, 1970).

A vessel-fitting algorithm was used to estimate vessel diameter (in pixels) and optical transmission of vessels (see Figure 4). Vessel diameter at 570nm was estimated according to the method described by Fischer et al., (Fischer et al., 2010), where the vessel boundaries are defined as the points in the vessel profile with the maximum rate of change in grayscale intensity. This provided reputable fitting for both bulbar conjunctival and episcleral vessels. Using this fitting algorithm, greyscale intensity in the centre of each vessel ( $I_v$ ) was calculated and the background greyscale intensity at the centre of the vessel ( $I_o$ ) was estimated by a linear fit to the background. OD was then calculated for each wavelength by:

$$OD_{\lambda} = -\log_{10} \left( \frac{I_v}{I_o} \right). \quad (1)$$

ODR, defined as  $ODR = OD_{560}/OD_{570}$ , was then calculated for each vessel; ODR is a direct proxy for  $SO_2$ ; if  $SO_2$  increases, ODR decreases. ODR is approximately independent of vessel diameter and concentration of hemoglobin.

If two or more reference  $SO_2$  values are known, then ODR can be empirically calibrated to  $SO_2$  (Beach et al., 1999). However, no calibration is possible for this study because no empirical measurements of  $SO_2$  in either bulbar conjunctival or episcleral vasculature have been reported in the literature, so we report results simply in terms of ODR.

### 3. RESULTS

#### 3.1 Sclera phantom

A total of eight *ex vivo* blood samples of various oxygenations were imaged and analysed in the scleral phantom. Some variation in ODR was seen as blood flowed along the capillary. Overall, ODR was found to decrease with increasing  $SO_2$  and the data was well fitted by a linear trend ( $R^2 = 0.89$ ) (see Figure 5), validating the use of our MSI technique for oximetry of vessels in a scleral-like configuration. Repeatability of scleral phantom ODR measurements was  $<0.5\%$  (standard deviation of 10 consecutive images).

### **3.2 Repeatability of *in vivo* ODR**

The repeatability of *in vivo* ODR measurements is summarised in Table 1. The greater repeatability of ODR measurement of bulbar conjunctival vessels (0.96%) compared to episcleral vessels (1.55%) when calculated as an average across vessel type is probably due to the larger number of bulbar conjunctival vessel sections analyzed (57 in total) compared to episcleral vessel sections (22 in total); the larger number of vessels analysed reduces the sensitivity to fluctuations in ODR.

### **3.4. Eyelid closure during normoxia**

Eyelid closure during normoxia resulted in no statistically significant change in ODR of either bulbar conjunctival or episcleral vessels. When the eyelid was open with the same gaze for 2.5 minutes, the average ODR was  $0.90 \pm 0.08$  (mean  $\pm$  standard deviation) for bulbar conjunctival vessels and  $0.94 \pm 0.09$  for episcleral vessels. After eyelid closure, average ODR was  $0.90 \pm 0.08$  for bulbar conjunctival vessels and  $0.93 \pm 0.08$  for episcleral vessels ( $p = 0.99, 0.72$  respectively; paired t-test).

### **3.5. Acute mild hypoxia**

Table 2 and Figure 6 summarise measurements of ODR, vessel diameter, and fingertip pulse oximetry at normoxia and hypoxia. Figure 6a shows ODR and pulse

oximeter data throughout the whole normoxia/hypoxia sequence. Bulbar conjunctival ODR increased with hypoxia (indicating a reduction in  $SO_2$ ) from  $0.846 \pm 0.014$  (mean  $\pm$  standard error) at normoxia to  $0.916 \pm 0.011$  at hypoxia ( $p < 0.001$ , paired t-test) (Figure 6b). Episcleral ODR increased on average, from  $0.881 \pm 0.019$  (mean  $\pm$  standard error) at normoxia to  $0.938 \pm 0.018$  at hypoxia ( $p = 0.03$ , paired t-test) (Figure 6c). Figure 7 shows an overlaid ODR map of vessels at normoxia and hypoxia.

Bulbar conjunctival vessel diameter did not change significantly between normoxia and hypoxia ( $p = 0.89$ , paired t-test), however increases in vessel diameters were apparent in some subjects, whereas decreases in diameters were seen in others (Figure 6d). Diameters of episcleral vessels were observed to increase from  $78.9 \pm 8.65\mu m$  (mean  $\pm$  standard deviation) at normoxia to  $97.6 \pm 14.3\mu m$  at hypoxia (Figure 6e) ( $p = 0.02$ , paired t-test).

### 3.6. Exposure of hypoxic vasculature to ambient air

For all eight datasets (four subjects, each imaged twice) ODR of hypoxic bulbar conjunctival vessels rapidly decreased upon eyelid opening (indicating an increase in  $SO_2$ ), tending asymptotically to an ODR corresponding to ODR measured at normoxia. The variation in ODR was well-fitted by an exponential-decay function representing re-oxygenation of the conjunctival vessels plus a linear component, reflecting the incoming hypoxic blood supply:

$$OD = a * e^{-bt} + ct + d \quad (2)$$

Where  $t$  is time and  $a$ ,  $b$ ,  $c$ ,  $d$ , are empirically calculated constants. The half-time to full reoxygenation ( $T_{1/2}$ ) can then be calculated by:

$$T_{1/2} = -\frac{\ln(2)}{b}. \quad (3)$$



$T_{1/2}$  varied on both an intra and inter-subject basis (see Table 3) but averaged over all measurements  $T_{1/2}$  was  $3.4 \pm 1.4$  seconds (mean  $\pm$  standard deviation). Figure 8 shows this reoxygenation process in two representative subjects.

Episcleral vessel ODR remained higher (i.e. lower  $SO_2$ ) after eyelid opening than at normoxia levels and was well fitted by a linear trend. Pulse oximeter  $SO_2$  followed a similar trend to episcleral ODR.

## **4. Discussion**

### **4.1. Validation of oximetry technique using scleral phantom**

Results from the scleral phantom measurement validated the ability of the spectral imaging technique to characterise ODR for oximetry for blood vessels. Some variation in ODR was observed when blood flowed through the capillaries; this variation is likely to be due to non-homogenous  $SO_2$  due to non-uniform deoxygenation by discrete crystals of Sodium Dithionite added to blood (Briley-Saebo and Bjornerud, 2000). Further variation in ODR may be caused by the aggregation of blood cells, which alters the optical path of light through blood. Nevertheless, the results shown in Figure 5 clearly support that ODR decreases with  $SO_2$ .

### **4.2. Effects of acute mild hypoxia**

In episcleral vessels, vessel diameter increased and  $SO_2$  decreased at acute mild hypoxia conditions. This is similar to auto-regulation of retinal vessels during acute mild hypoxia (Choudhary et al., 2013). In bulbar conjunctival vessels,  $SO_2$  also decreased with hypoxia, but average vessel diameter did not change significantly. This confirms that the increase in ODR observed is due a decrease in  $SO_2$  and not due a secondary effect due to change of vessel diameter.

### 420 4.3. Consequences of oxygen diffusion

421 Our study is the first to directly show that oxygen diffusion from air results in rapid  
422 reoxygenation and saturation of hypoxic bulbar conjunctival vessels. This  
423 measurement would not be possible with Clark electrodes, which are limited to a  
424 single point measurement and crucially, block oxygen diffusion between ambient air  
425 and the tissue in measurement. Hill and Fatt (1963) did however use a Clarke  
426 electrode to demonstrate that the bulbar conjunctiva would uptake oxygen from a  
427 limited  $pO_2$  reservoir via diffusion, concluding that oxygen diffusion from ambient air  
428 to the exposed bulbar conjunctival vessels occurs constantly (Hill and Fatt, 1963).  
429 This study is the first to directly observe how this oxygen diffusion alters bulbar  
430 conjunctival  $SO_2$ .

431

432 It is expected that when in equilibrium with ambient air ( $pO_2 \sim 160\text{mmHg}$ ), bulbar  
433 conjunctival vessels will be close to 100%  $SO_2$  because normal arterial blood ( $\sim 95$ -  
434  $97\%$   $SO_2$ ) corresponds to a typical  $pO_2$  of 80-100mmHg; much less than 160mmHg  
435 (Verma and Roach, 2010; Williams, 1998). The average ODR was of exposed  
436 bulbar conjunctival vessels was consistently  $\sim 0.95$  (see Figure 6a), indicating a  
437 constant equilibrium as expected.

438

439 In retinal oximetry, ODR is often empirically calibrated to  $SO_2$  by assuming retinal  
440 arterial  $SO_2$  to be equal to the systemic arterial  $SO_2$  as measured by a pulse  
441 oximeter. Our results show that the oxygen dynamics of episcleral vessels are  
442 similar to pulse oximetry, so this calibration approach would be valid for episcleral  
443 vessels *if* arteries and veins could be accurately identified. However, this calibration  
444 approach would not work for bulbar conjunctival vessels because our results show

that the oxygen dynamics of bulbar conjunctival vessels do not reflect the oxygen dynamics of systemic arterial  $SO_2$

#### **4.4. Challenges of bulbar conjunctival and episcleral oximetry**

In the retina, oximetry results are often reported independently for arterioles and venules. However, in this study we report results for generalised vasculature and not separately as arterioles and venules for several reasons. (1) Bulbar conjunctival arterioles and venules could not be reliably distinguished from morphology alone due to the significant variation in bulbar conjunctival vessel morphology (Meighan, 1956). (2) Bulbar conjunctival vessels will be highly oxygenated when exposed to ambient air due to oxygen diffusion from air, and thus could not be distinguished on the basis of ODR. (3) The relatively low number of episcleral vessels that met inclusion criteria did not allow sufficient comparison to identify arteries and veins by either vessel morphology or ODR. Reliable discrimination between episcleral arteries and veins could however be achieved with fluorescence angiography (Ormerod et al., 1995).

Rattlesnaking - a false apparent change in ODR along the length of a vessel section - is a common artefact in two-wavelength oximetry. Rattlesnaking was observed in both bulbar conjunctival and episcleral vessels and can be seen in Figure 7.

Rattlesnaking may be caused by a number of factors such as nearby vessels, variations in scattering properties of background tissue, and groups of erythrocytes flowing in vessels. In small vessels, rattlesnaking may be enhanced in magnitude by the small numbers of red blood cells flowing through narrow vessels.

In this study, only the immediate repeatability of oximetry measurements was assessed. In future, quantifying the repeatability of measurements over the course of an entire day would be useful because fluctuating diurnal variation in vessel diameter

and temperature of bulbar conjunctival vessels has been reported (Duench et al., 2007).

#### **4.5. Influence of light scattering by scleral tissue**

Optical scattering of light by tissue may influence ODR and vessel diameter measurement. We assume negligible scattering for the bulbar conjunctival vasculature, which lies within a thin ( $\sim 33\mu\text{m}$ ), transparent bulbar conjunctiva (Efron et al., 2009). However, episcleral vessels are embedded in scleral tissue; this will affect our measurement in two ways. Firstly, the sharpness of vessel boundaries may be decreased, which may reduce the accuracy of vessel diameter measurement for episcleral vessels. However, the relative change in vessel diameter measured will should still be accurate. Secondly, scattering from overlying tissue will act to reduce contrast of vessels, generally acting to reduce the changes in ODR observed. Scattering will also be increased if vessels dilate; this will reduce the apparent change in ODR of episcleral vessels which were observed to dilate significantly (see Figure 6e). In the scleral phantom, the FEP plastic of the capillary will contribute to scattering. The challenge of light scattering by tissue and within blood and the absence of reliable  $\text{SO}_2$  values for calibration, makes absolute oximetry in bulbar conjunctival and episcleral vessels challenging, however, as we describe here, changes in  $\text{SO}_2$  can be robustly characterised with ODR and can provide useful biological insight.

#### **4.6. Future work**

There are good prospects of achieving an absolute oximetry, with minimal requirement for calibration by incorporating the modified Beer-Lambert law (Delpy et al., 1988; Pittman and Duling, 1975) into multi-waveband optical transmission models. Absolute oximetry would be of particular use because there have been no

reference values for  $\text{SO}_2$  of the bulbar conjunctival or episcleral microvasculature reported in the literature, so two wavelength oximetry cannot be accurately calibrated.

With appropriate flash illumination, imaging at 100Hz or greater could be achieved and oximetry in smaller bulbar conjunctival vessels and capillaries could be enabled by adapting a slit lamp for high-magnification multispectral imaging. This could enable the potential for non-contact oximetry of groups of red blood cells in humans *in vivo*. Individual red blood cell oximetry has previously been achieved *ex vivo* using SMSI (Fernandez Ramos et al., 2014) and invasively *in vivo* in anaesthetised mice by photoacoustic microscopy (Wang et al., 2013). SMSI offers faster image acquisition and a simpler image system compared to PAM.

#### **4.7. Vascular conditions that may affect anterior segment vessel $\text{SO}_2$**

Understanding  $\text{SO}_2$  of bulbar conjunctival and episcleral vessels may provide insight into a range of conditions. For example, diabetic retinopathy is known to result in increased retinal vessel  $\text{SO}_2$  (Hammer et al., 2009; Hardarson and Stefánsson, 2012), however, previous studies have shown that oxygen tension in diabetic subjects is lower than in healthy controls (Isenberg et al., 1986). Further, diabetes is associated with increased bulbar conjunctival vessel diameter (Cheung, Anthony T. W. Ramanujam et al., 2001), capillary loss (Owen et al., 2008), and decreased vessel reactivity (Fenton et al., 1979). Snapshot multispectral-imaging oximetry could also provide direct *in vivo* measurement of resultant hypoxia in bulbar conjunctival vasculature from contact lens wear (Heitmar et al., 2012; Sweeney, 2013). Furthermore oximetry of the bulbar conjunctival vessels may be of interest in studying the recovery of ocular burns using oxygen therapy (Sharifipour et al., 2011), recovery of circulation after surgical or traumatic wound healing, and possibly in the

study of ischemic conditions such as dry-eye syndrome (Menezo and Lightman, 2004). High intra-ocular pressure (IOP) is associated with narrowed episcleral veins and increased diameter of episcleral arteries (Nanba and Schwartz, 1986), but it is not known if this may alter episcleral  $SO_2$ .

## 5. Conclusions

This is the first study to quantify changes localised in  $SO_2$  of bulbar conjunctival and episcleral microvasculature. Oximetry was achieved using SMSI and was validated using a sclera-mimicking phantom.

*In vivo*, acute mild hypoxia resulted in a repeatable reduction in  $SO_2$  of both bulbar conjunctival and episcleral microvasculature. Episcleral vessels were observed to dilate due to acute mild hypoxia, whereas bulbar conjunctival vessels did not show statically significant dilation under hypoxia. Hypoxic bulbar conjunctival vessels were observed to rapidly reoxygenate due to oxygen diffusion when exposed to ambient air. Episcleral vessels were not observed to reoxygenate due to overlying episcleral tissue. This oxygen diffusion means that after exposure to air, the  $pO_2$  of bulbar conjunctival vessels will be in equilibrium with ambient air, resulting in a  $SO_2$  close to 100%. SMSI is currently the only oximetry technique with sufficient spatiotemporal resolution to measure this rapid oxygen diffusion in individual vessels. However we have shown that the role of oxygen diffusion in the bulbar conjunctiva must be considered for any future oximetry studies to provide meaningful results.

SMSI oximetry of the bulbar conjunctival and episcleral microvasculature may be of interest in investigating oxygen dynamics in a variety of microvasculature conditions where hypoxia may play a role, such as diabetes, (Isenberg et al., 1986; Hammer et

al., 2009; Hardarson and Stefánsson, 2012), sickle-cell disease (Isenberg et al., 1987), dry-eye syndrome (Menezo and Lightman, 2004), contact lens wear (Heitmar et al., 2012; Sweeney, 2013), high intra-ocular pressure (Nanba and Schwartz, 1986), traumatic or surgical wound healing, and ocular-burn recovery (Sharifipour et al., 2011). Further, high-magnification MSI of the bulbar conjunctiva could enable non-invasive *in vivo* oximetry of individual red blood cells.

## References

- Alabboud, I., Muyo, G., Gorman, A., Mordant, D., McNaught, A., Petres, C., Petillot, Y.R., Harvey, A.R., 2007. New spectral imaging techniques for blood oximetry in the retina. *Proc. SPIE 6631, Nov. Opt. Instrum. Biomed. Appl. III 6631*. doi:10.1117/12.728535
- Bashkatov, A.N., Genina, E.A., Kochubey, V.I., Tuchin, V. V., 2010. Optical properties of human sclera in spectral range 370-2500 nm. *Opt. Spectrosc.* 109, 197–204. doi:10.1134/S0030400X10080084
- Beach, J.M., Schwenzer, K.J., Srinivas, S., Kim, D., Tiedeman, J.S., 1999. Oximetry of retinal vessels by dual-wavelength imaging: calibration and influence of pigmentation. *JAP* 86, 748–758.
- Boeckeaert, J., Vandewalle, E., Stalmans, I., 2012. Oximetry: recent insights into retinal vasopathies and glaucoma. *Bull. Soc. Belge Ophtalmol.* 75–83.
- Briley-Saebo, K., Bjornerud, A., 2000. Accurate de-oxygenation of ex vivo whole blood using sodium dithionite. *Proc. Intl. Soc. Mag. Reson. Med* 2025.
- Chapman, K.R., Liu, F.L., Watson, R.M., Rebuck, A.S., 1986. Conjunctival oxygen tension and its relationship to arterial oxygen tension. *J. Clin. Monit.* 2, 100–104.
- Cheung, A., Hu, B., Wong, S., Chow, J., Chan, M., To, W., Li, J., Ramanujam, S., Chen, P., 2012. Microvascular abnormalities in the bulbar conjunctiva of contact

580 lens users. *Clinical hemerology Microcirc.* 51, 77–86. doi:10.3233/CH-2011-  
581 1513.

582 Cheung, Anthony T. W. Ramanujam, S., Greer, D.A., Kumagai, L.F., Aoki, T.T.,  
583 2001. Microvascular abnormalities in the bulbar conjunctiva of patients with type  
584 2 diabetes. *Endocr. Pract.* 7, 358–363.

585 Choudhary, T.R., Ball, D., Fernandez Ramos, J., McNaught, A.I., Harvey, A.R.,  
586 2013. Assessment of acute mild hypoxia on retinal oxygen saturation using  
587 snapshot retinal oximetry. *Invest. Ophthalmol. Vis. Sci.* 54, 38–43.  
588 doi:10.1167/iovs.13-12624

589 Crihalmeanu, S., Ross, A., 2012. Multispectral scleral patterns for ocular biometric  
590 recognition. *Pattern Recognit. Lett.* 33, 1860–1869.  
591 doi:10.1016/j.patrec.2011.11.006

592 Delpy, D.T., Cope, M., van der Zee, P., Arridge, S., Wray, S., Wyatt, J., 1988.  
593 Estimation of optical pathlength through tissue from direct time of flight  
594 measurement. *Phys. Med. Biol.* 33, 1433–1442. doi:10.1088/0031-  
595 9155/33/12/008

596 Duench, S., Simpson, T., Jones, L.W., Flanagan, J.G., Fonn, D., 2007. Assessment  
597 of variation in bulbar conjunctival redness, temperature, and blood flow. *Optom.*  
598 *Vis. Sci.* 84, 511–556. doi:10.1097/OPX.0b013e318073c304

599 Efron, N., Al-Dossari, M., Pritchard, N., 2009. In vivo confocal microscopy of the  
600 bulbar conjunctiva. *Clin. Experiment. Ophthalmol.* 37, 335–344.  
601 doi:10.1016/j.jfma.2013.10.003

602 Eliasdottir, T.S., Bragason, D., Hardarson, S.H., Kristjansdottir, G., Stefánsson, E.,  
603 2014. Venous oxygen saturation is reduced and variable in central retinal vein  
604 occlusion. *Graefe's Arch. Clin. Exp. Ophthalmol.* doi:10.1007/s00417-014-2849-  
605 2

606 Fenton, B.M., Zweifach, B.W., Worthen, D.M., 1979. Quantitative morphometry of



607 conjunctival microcirculation in diabetes mellitus. *Microvasc. Res.* 18, 153–166.  
 608 doi:10.1016/0026-2862(79)90025-6  
 609 Fernandez Ramos, J., Brewer, L.R., Gorman, A., Harvey, A.R., 2014. Video-rate  
 610 multispectral imaging: application to microscopy and macroscopy. *Opt. Soc. Am.*  
 611 doi:10.1364/COSI.2014.CW1C.3  
 612 Fischer, M.J.M., Uchida, S., Messlinger, K., 2010. Measurement of meningeal blood  
 613 vessel diameter in vivo with a plug-in for ImageJ. *Microvasc. Res.* 80, 258–266.  
 614 doi:10.1016/j.mvr.2010.04.004  
 615 Gartner, S., 1944. Blood vessels of the conjunctiva, studies with high speed  
 616 macrophotography. *Arch. Ophthalmol.* 32, 464–476. doi:  
 617 doi:10.1001/archopht.1944.00890120044004  
 618 Gorman, A., Fletcher-Holmes, D.W., Harvey, A.R., 2010. Generalization of the Lyot  
 619 filter and its application to snapshot spectral imaging. *Opt. Express* 18, 5602–8.  
 620 doi:10.1364/OE.18.005602  
 621 Hammer, M., Vilser, W., Riemer, T., Liemt, F., Jentsch, S., Dawczynski, J.,  
 622 Schweitzer, D., 2011. Retinal venous oxygen saturation increases by flicker light  
 623 stimulation. *Invest. Ophthalmol. Vis. Sci.* 52, 274–7. doi:10.1167/iovs.10-5537  
 624 Hammer, M., Vilser, W., Riemer, T., Mandecka, A., Schweitzer, D., Kühn, U.,  
 625 Dawczynski, J., Liemt, F., Strobel, J., 2009. Diabetic patients with retinopathy  
 626 show increased retinal venous oxygen saturation. *Graefes Arch. Clin. Exp.*  
 627 *Ophthalmol.* 247, 1025–30. doi:10.1007/s00417-009-1078-6  
 628 Hardarson, S.H., Harris, A., Karlsson, R.A., Halldorsson, G.H., Kagemann, L.,  
 629 Rechtman, E., Zoega, G.M., Eysteinnsson, T., Benediktsson, J.A., Thorsteinsson,  
 630 A., Jensen, P.K., Beach, J., Stefánsson, E., 2006. Automatic retinal oximetry.  
 631 *Invest. Ophthalmol. Vis. Sci.* 47, 5011–6. doi:10.1167/iovs.06-0039  
 632 Hardarson, S.H., Stefánsson, E., 2012. Retinal oxygen saturation is altered in  
 633 diabetic retinopathy. *Br. J. Ophthalmol.* 96, 560–3. doi:10.1136/bjophthalmol-

634 2011-300640

635 Harvey, A.R., Fletcher-Holmes, D.W., Gorman, A., Altenbach, K., Arlt, J., Read,  
636 N.D., 2005. Spectral imaging in a shapshot. *Proc. SPIE. Spectr. Imaging*  
637 *Instrumentation, Appl. Anal. III* 5694, 110–119. doi:10.1117/12.604609

638 Heitmar, R., Wright, S., Mousavi, M., Wolffsohn, J.S., 2012. Oxygen saturation  
639 measurements of the limbal vasculature before and after soft contact lens wear.  
640 *Contact Lens Anterior Eye* 35 S1, e19. doi:doi:10.1016/j.clae.2012.08.060

641 Hill, R., Fatt, I., 1963. Oxygen depletion of a limited resovoir by human conjunctiva.  
642 *Lett. to Nat.* doi:10.1038/2001011b0

643 Iguchi, S., Mitsubayashi, K., Uehara, T., Ogawa, M., 2005. A wearable oxygen  
644 sensor for transcutaneous blood gas monitoring at the conjunctiva. *Sensors*  
645 *Actuators B Chem.* 108, 733–737. doi:10.1016/j.snb.2004.12.099

646 Isenberg, S., Neumann, D., Fink, S., Rich, R., 2002. Continuous oxygen monitoring  
647 of the conjunctiva in neonates. *J. Perinatol.* 22, 46–49.  
648 doi:10.1038/sj/jp/7210602

649 Isenberg, S.J., Mcree, W.E., Jedrzynski, M., 1986. Conjunctival hypoxia in diabetes  
650 mellitus. *Invest. Ophthalmol. Vis. Sci.* 27, 1512–1515.

651 Isenberg, S.J., McRee, W.E., Jedrzynski, M.S., Gange, S.N., Gange, S.L., 1987.  
652 Effects of sickle cell anemia on conjunctival oxygen tension and temperature.  
653 *Arch. Intern. Med.* 147, 67–69. doi:10.1016/0736-4679(87)90250-2

654 Jiang, H., Ye, Y., Cabrera, D., Lam, B.L., Rundek, T., Tao, A., Shao, Y., Wang, J.,  
655 2013. Human conjunctival microvasculature assessed with a retinal function  
656 imager ( RFI ). *Microvasc. Res.* 85, 134–137. doi:10.1016/j.mvr.2012.10.003

657 Jiang, H., Zhong, J., DeBuc, D.C., Tao, A., Xu, Z., Lam, B.L., Liu, C., Wang, J.,  
658 2014. Functional slit lamp biomicroscopy for imaging bulbar conjunctival  
659 microvasculature in contact lens wearers. *Microvasc. Res.* 92, 62–71.  
660 doi:10.1016/j.mvr.2014.01.005

661 Kwan, M., Fatt, I., 1971. A noninvasive method of continuous arterial oxygen tension  
 662 estimation from measured palpebral conjunctival oxygen tension.  
 663 *Anesthesiology* 35.

664 Labsphere Inc., n.d. Optical-Grade Spectralon® Diffuse Reflectance Material  
 665 Specially Fabricated for Optical Components [WWW Document]. URL  
 666 [https://www.labsphere.com/wp-content/uploads/2015/06/Spectralon-Optical-](https://www.labsphere.com/wp-content/uploads/2015/06/Spectralon-Optical-Grade.pdf)  
 667 [Grade.pdf](https://www.labsphere.com/wp-content/uploads/2015/06/Spectralon-Optical-Grade.pdf) (accessed 11.4.15).

668 Mader, T.H., Friedl, K.E., Mohr, L.C., Bernhard, W.N., 1987. Conjunctival oxygen  
 669 tension at high altitude. *Aviat. Space. Environ. Med.* 58, 767–769.

670 Meighan, S.S., 1956. Blood vessels of the bulbar conjunctiva in man. *Br. J.*  
 671 *Ophthalmology* 40, 513–526.

672 Menezo, V., Lightman, S., 2004. The eye in systemic vasculitis. *Clin Med* 4, 250–  
 673 254. doi:10.1016/S0140-6736(04)17554-5

674 Mordant, D.J., Al-Abboud, I., Muyo, G., Gorman, A., Harvey, A.R., McNaught, A.I.,  
 675 2014. Oxygen saturation measurements of the retinal vasculature in treated  
 676 asymmetrical primary open-angle glaucoma using hyperspectral imaging. *Eye*  
 677 (Lond). 28, 1190–200. doi:10.1038/eye.2014.169

678 Mordant, D.J., Al-Abboud, I., Muyo, G., Gorman, A., Sallam, A., Ritchie, P., Harvey,  
 679 a R., McNaught, a I., 2011. Spectral imaging of the retina. *Eye* 25, 309–20.  
 680 doi:10.1038/eye.2010.222

681 Mordant, D.J., Al-Abboud, I., Muyo, G., Gorman, A., Sallam, A., Rodmell, P., Crowe,  
 682 J., Morgan, S., Ritchie, P., Harvey, A.R., McNaught, A.I., 2011. Validation of  
 683 human whole blood oximetry, using a hyperspectral fundus camera with a model  
 684 eye. *Invest. Ophthalmol. Vis. Sci.* 52, 2851–9. doi:10.1167/iovs.10-6217

685 Nanba, K., Schwartz, B., 1986. Increased diameter of the anterior ciliary artery with  
 686 increased intraocular pressure. *Arch Ophthalmol* 104, 1652–1655.  
 687 doi:10.1001/archopht.1986.01050230090039

688 Olafsdottir, O.B., Hardarson, S.H., Gottfredsdottir, M.S., Harris, A., Stefánsson, E.,  
 689 2011. Retinal oximetry in primary open-angle glaucoma. *Invest. Ophthalmol.*  
 690 *Vis. Sci.* 52, 6409–13. doi:10.1167/iovs.10-6985  
 691 Ormerod, L.D., Fariza, E., Webb, R.H., 1995. Dynamics of external ocular blood flow  
 692 studied by scanning angiographic microscopy. *Eye* 9, 605–614.  
 693 Owen, C.G., Newsom, R.S.B., Rudnicka, A.R., Barman, S.A., Woodward, E.G., Ellis,  
 694 T.J., 2008. Diabetes and the tortuosity of vessels of the bulbar conjunctiva.  
 695 *Ophthalmology* 115, e27–e32. doi:doi:10.1016/j.opthta.2008.02.009  
 696 Pittman, R., Duling, B., 1975. A new method for the measurement of percent  
 697 oxyhemoglobin. *J. Appl. Physiol.* 38.  
 698 Prael, S., 1999. Optical absorption of hemoglobin [WWW Document]. Oregon Med.  
 699 Laser Cent.  
 700 Shahidi, M., Wanek, J., Gaynes, B., Wu, T., 2010. Quantitative assessment of  
 701 conjunctival microvascular circulation of the human eye. *Microvasc. Res.* 79,  
 702 109–13. doi:10.1016/j.mvr.2009.12.003  
 703 Sharifipour, F., Baradaran-Rafii, A., Idani, E., Zamani, M., Jabbarpoor Bonyadi, M.H.,  
 704 2011. Oxygen therapy for acute ocular chemical or thermal burns: a pilot study.  
 705 *Am. J. Ophthalmol.* 151, 823–828. doi:10.1016/j.ajo.2010.11.005  
 706 Spurling, K.J., Zammit, C., Lozewicz, S., 2011. Mains-powered hypoxic gas  
 707 generation: a cost-effective and safe method to evaluate patients at risk from  
 708 hypoxia during air travel. *Thorax* 66, 731–2. doi:10.1136/thx.2010.141655  
 709 Sweeney, D., 2013. Have silicone hydrogel lenses eliminated hypoxia? *Eye Contact*  
 710 *Lens Sci. Clin. Pract.* 39, 53–60. doi:10.1097/ICL.0b013e31827c7899  
 711 van Assendelft, O.W., 1970. Spectrophotometry of haemoglobin derivatives. Van  
 712 Gorcum.  
 713 van Zijderveld, R., Ince, C., Schlingemann, R.O., 2014. Orthogonal polarization  
 714 spectral imaging of conjunctival microcirculation. *Graefes Arch. Clin. Exp.*

715 Ophthalmol. doi:10.1007/s00417-014-2603-9  
716 Verma, A., Roach, P., 2010. The interpretation of arterial blood gases. *Aust. Prescr.*  
717 33, 124–129.  
718 Wanek, J., Gaynes, B., Lim, J.I., Molokie, R., Shahidi, M., 2013. Human bulbar  
719 conjunctival hemodynamics in hemoglobin SS and SC disease. *Am. J. Hematol.*  
720 88, 661–664. doi:10.1002/ajh.23475  
721 Wang, L., Maslov, K., Wang, L. V, 2013. Single-cell label-free photoacoustic  
722 flowoxigraphy in vivo. *Proc. Natl. Acad. Sci. U. S. A.* 2013, 1–6.  
723 doi:10.1073/pnas.1215578110  
724 Williams, A.J., 1998. Assessing and interpreting arterial blood gases and acid-base  
725 balance. *Br. Med. J.* 317, 1213–1216.  
726

## 727 **Acknowledgements**

728 This work was supported by the University of Glasgow Sensors Initiative.  
729 Disclosure: L.E. MacKenzie, None; T.R. Choudhary, None; A.I. McNaught, None;  
730 A.R. Harvey, None.  
731

**Figure 1 (a)** Simplified diagram showing position of bulbar conjunctival and episcleral vasculature with respect to the sclera and ambient air. **(b)** Representative image of vasculature observed when imaging the sclera. Bulbar conjunctival vessels are marked with white arrows and episcleral vessels are marked with yellow dashed diamond arrows.

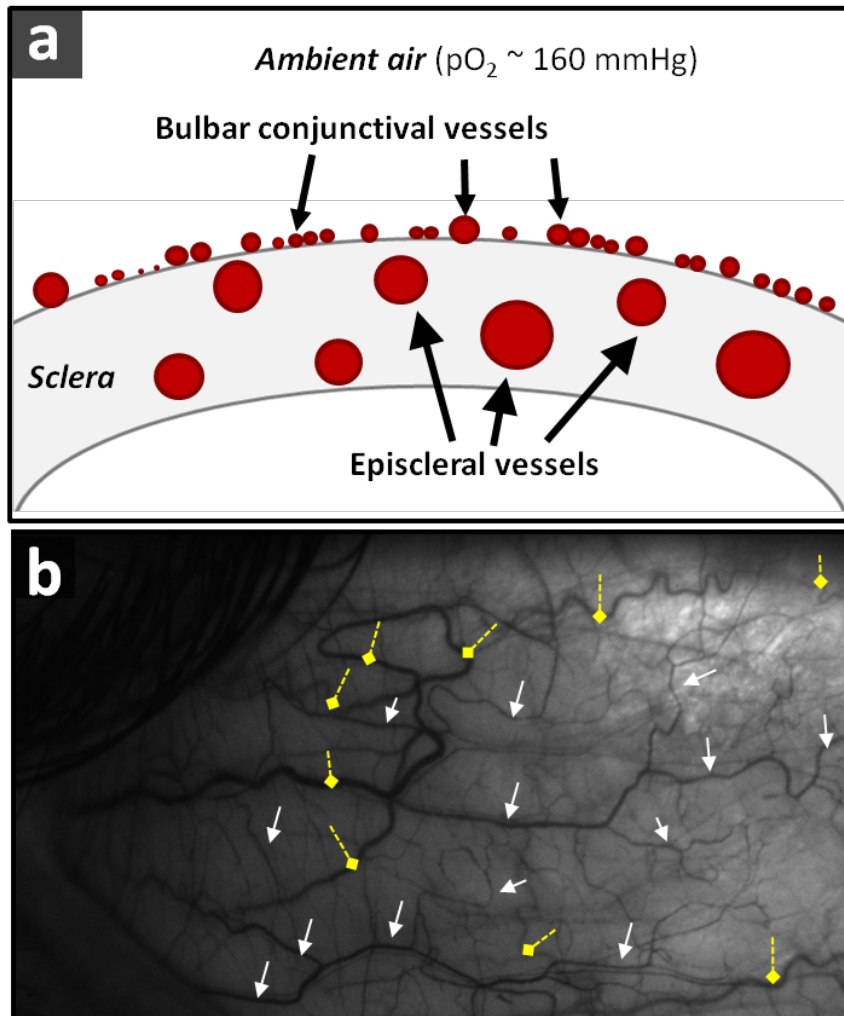


**Figure 2 (a)** The imaging system: a commercial fundus camera with the Image Replicating Imaging Spectrometer (IRIS) fitted to the upper imaging port. **(b)** A representative 8-band IRIS image of bulbar conjunctival and episcleral vasculature.

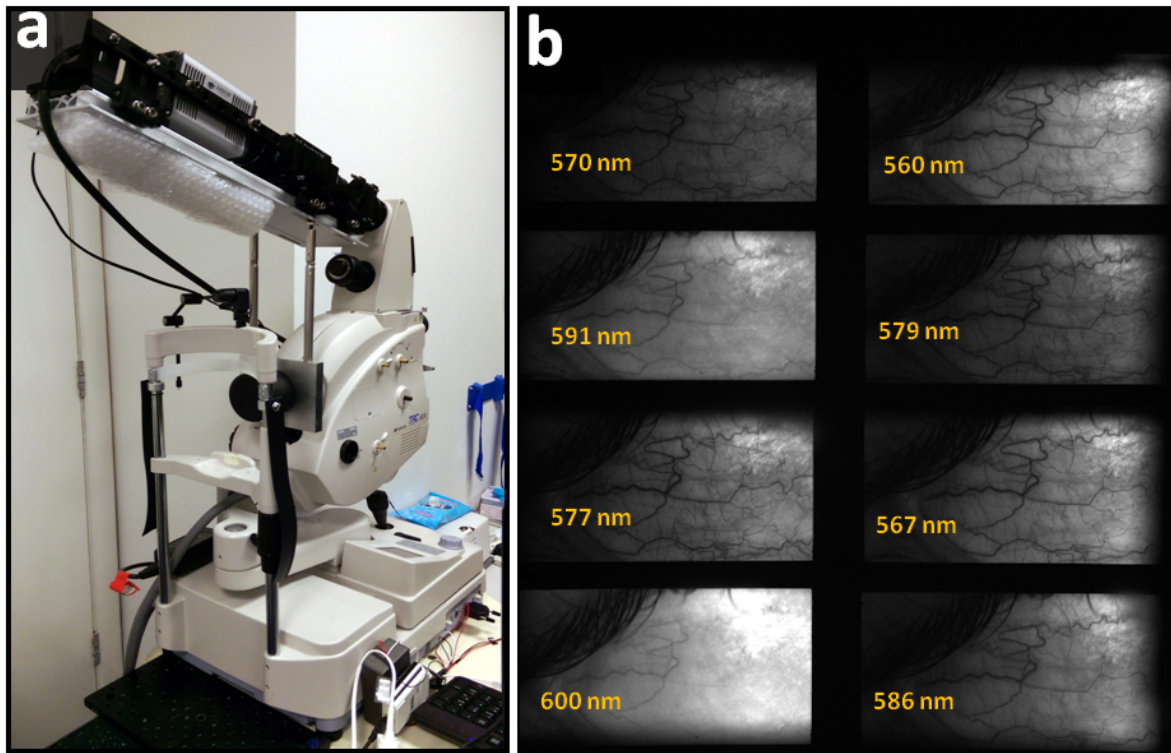


**Figure 3. (a)** diagram of the scleral phantom. **(b)** 100 $\mu$ m capillary filled with blood; scale bar represents one millimetre.

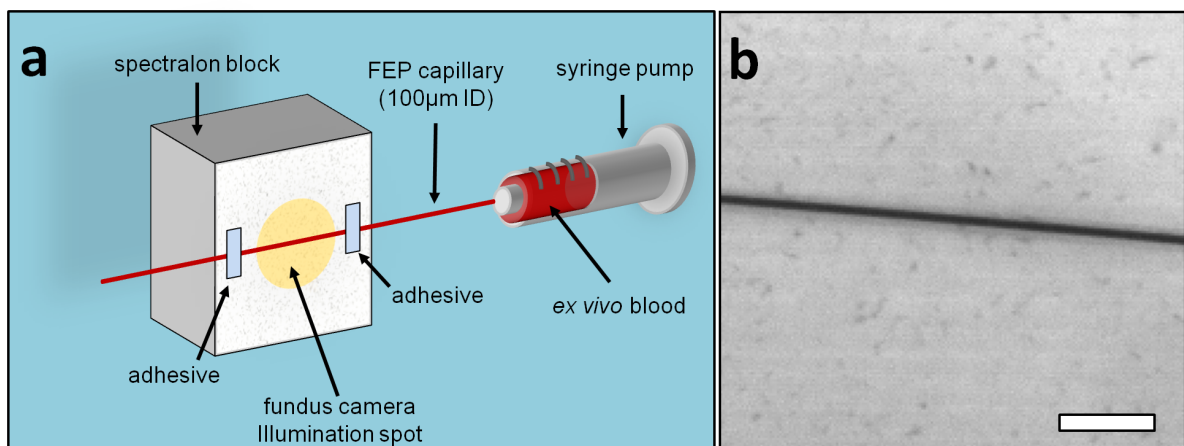


**Figure 4.** Depiction of the vessel fitting algorithm applied to estimate vessel diameter, the greyscale intensity in centre of vessel ( $I_v$ ), and the background greyscale intensity ( $I_o$ ). Vessel boundaries are defined as the points of maximum rate of change of grayscale intensity in the vessel profile.

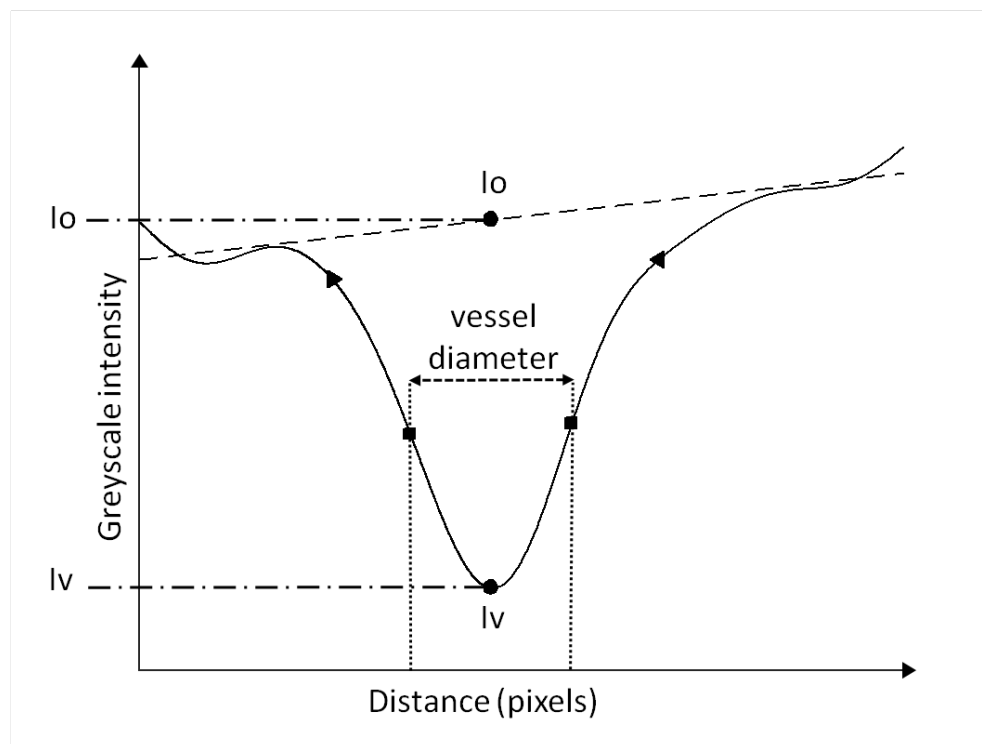


**Table 1.** Repeatability of optical-density ratio (ODR) measurements for conjunctival and episcleral vessels.

Parameter	Bulbar Conjunctival vessels	Episcleral vessels
Number of subjects	10	7
Total number of sampled vessel sections	57	22
ODR repeatability: individual vessels*	2.27%	2.28%
ODR repeatability**	0.96%	1.55%

\*standard deviation of 8 repeated measurements of individual vessels, averaged across all subjects

\*\* standard deviation of the average ODR of vessels when averaged by vessel type, then averaged across all subjects



**Table 2.** Average optical-density ratio (ODR), diameter of vessels, and pulse oximeter data at normoxia and hypoxia.

Parameter	Number of subjects	Number of vessel sections analysed	Normoxia	Hypoxia	p-value*
<b>Conjunctival ODR</b> (mean ± SE)	10	64	0.846 ± 0.014	0.916 ± 0.011	<0.001
<b>Episcleral ODR</b> (mean ± SE)	7	24	0.880 ± 0.019	0.938 ± 0.018	0.03
<b>Conjunctival diameter (µm)</b> (mean ± SD)	10	64	80.1 ± 7.6	80.6 ± 7.0	0.89
<b>Episcleral diameter (µm)</b> (mean ± SD)	7	24	78.9 ± 8.7	97.6 ± 14.3	0.02
<b>Fingertip pulse oximeter SO<sub>2</sub> (%)</b> (mean ± SD)	10	N/A	97.1 ± 1.7	86.7 ± 4.3	<0.001

\*Pairwise t-test

SE = standard error

SD = standard deviation

**Figure 5.** Phantom validation; optical-density ratio (ODR) was measured to be inversely proportional to  $\text{SO}_2$  as measured by a blood gas analyser (BGA). Vertical error bars represent standard deviation of ODR as measured along the length of the FEP capillary, horizontal error bars represent the blood gas analyser manufacturers quoted error of  $\pm 1.8\%$   $\text{SO}_2$ . Dashed line is fitted linear trend ( $R^2 = 0.89$ ).

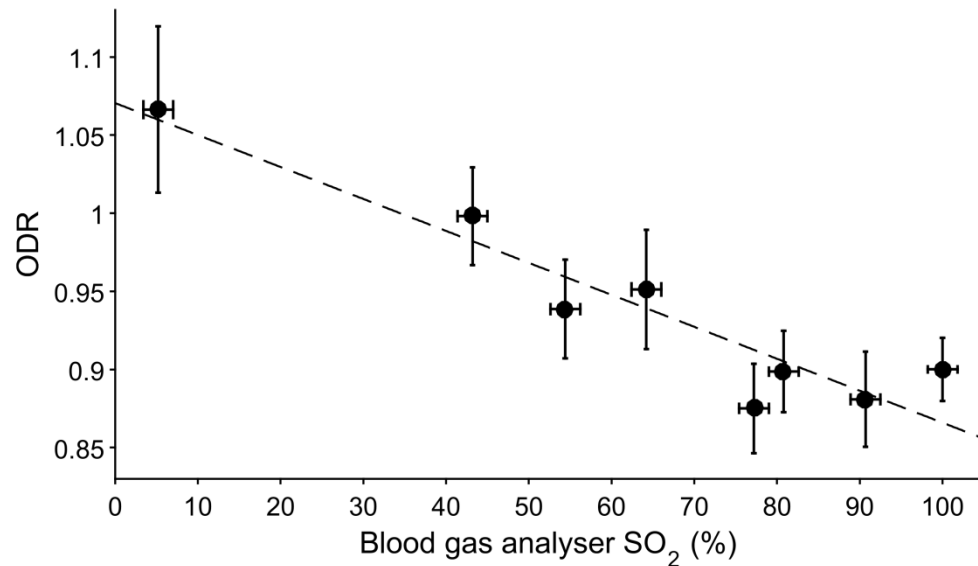


**Figure 6. (a)** Average optical-density ratio (ODR) and pulse oximeter data throughout the normoxia/hypoxia sequence. Error bars are the standard error of the mean. Graphs **(b)-(e)** show pairwise change of average vessel diameter and average ODR for each subject at normoxia and hypoxia. Statistically significant results are denoted with an asterisk (\*).

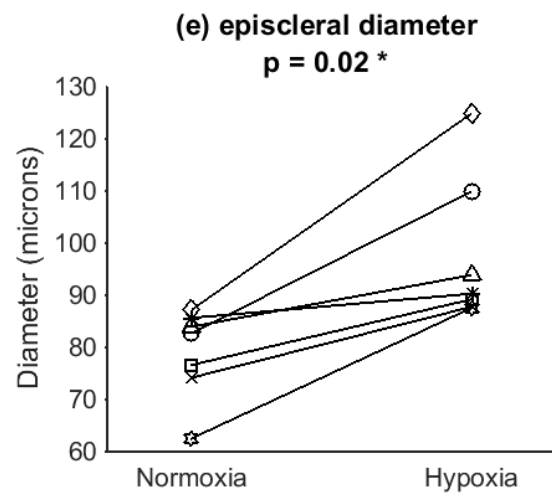
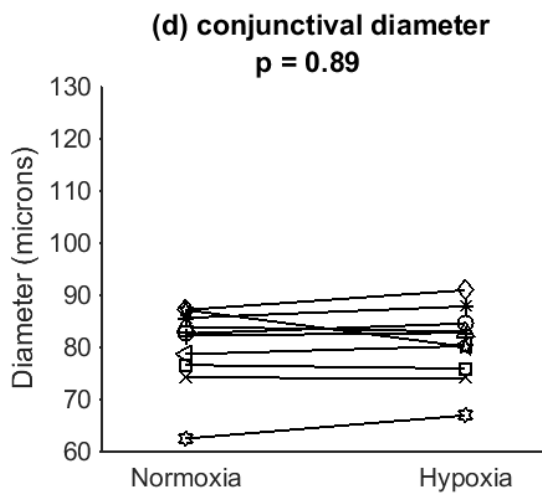
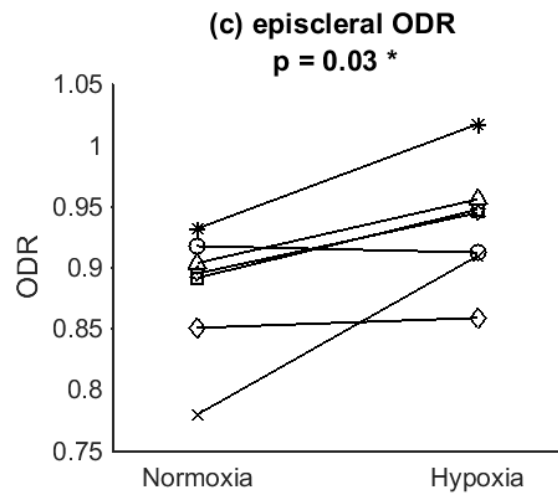
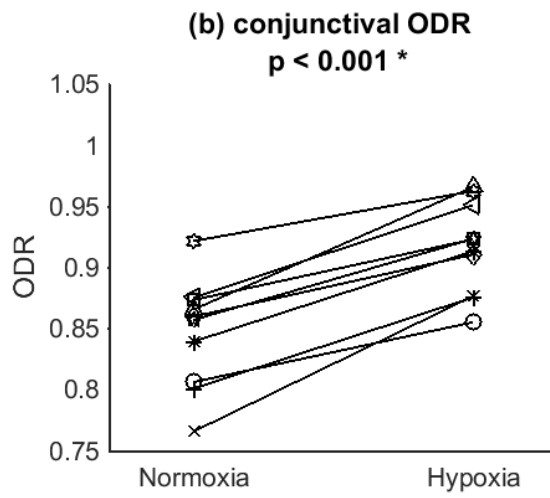
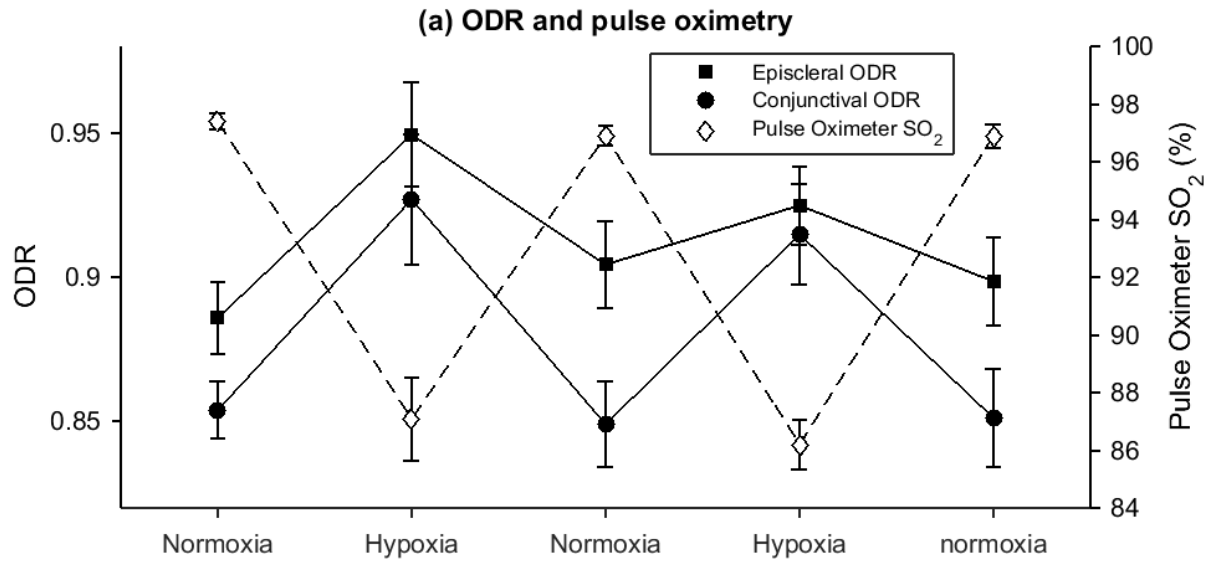
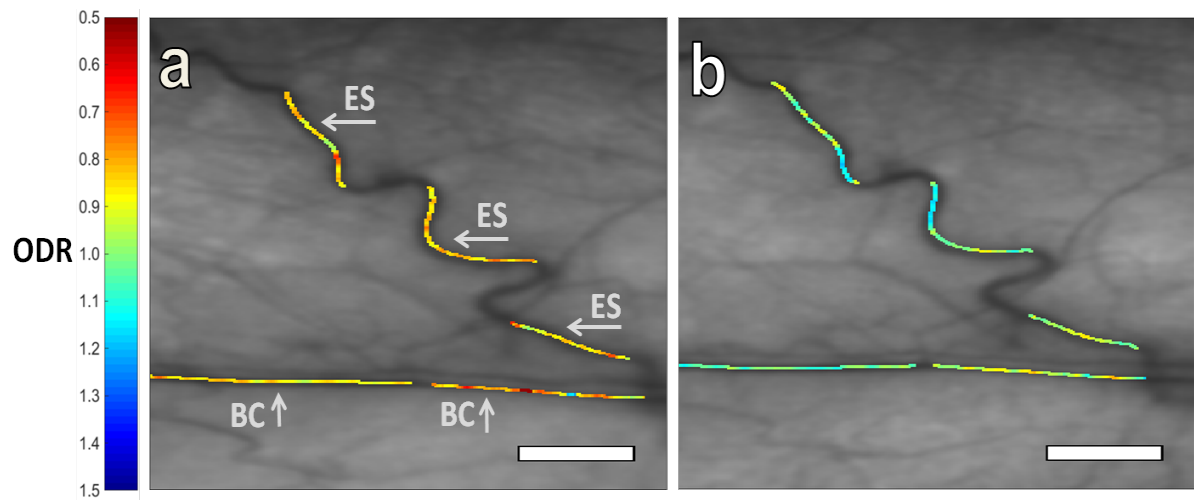
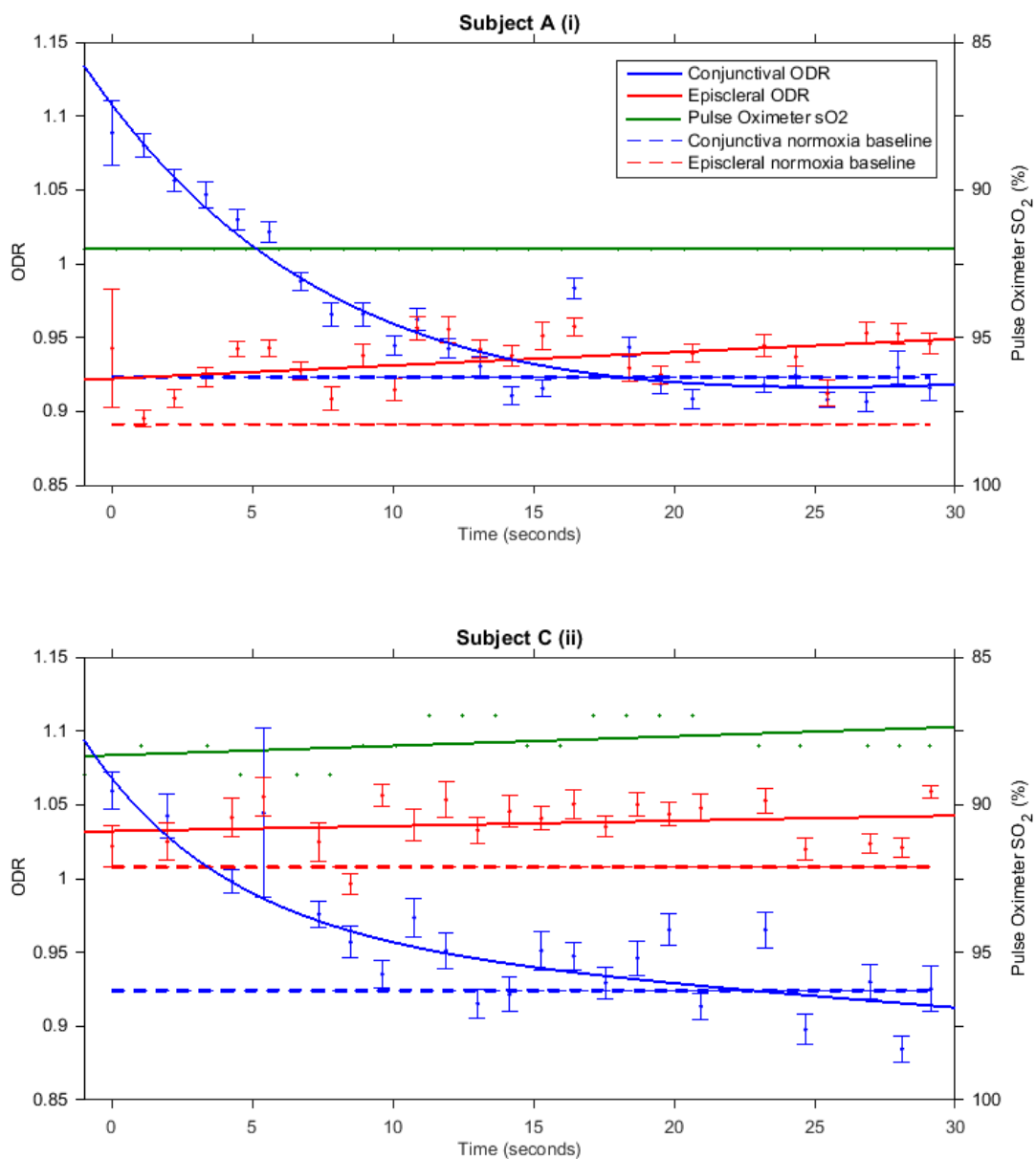


**Figure 7.** Optical-density ratio (ODR) map of vasculature at **(a)** normoxia and **(b)** hypoxia. ODR increases (i.e.  $\text{SO}_2$  decreases) with hypoxia. Episcleral vessels are labelled with (ES) and bulbar conjunctival vessels are labelled (BC). Scale bar represents 500  $\mu\text{m}$ .



800

801 **Figure 8.** Optical-density ratio (ODR) of hypoxic vasculature versus time after eyelid  
 802 opening (i.e. exposure to ambient air) in two representative subjects. Bulbar  
 803 conjunctival ODR (blue fitted line) decreased exponentially upon eyelid opening  
 804 before reaching normoxia baseline levels (blue dashed line). Episcleral ODR (red  
 805 fitted line) remained higher than normoxia levels (red dashed line). This indicates  
 806 that hypoxic bulbar conjunctival vessels rapidly reoxygenated by oxygen diffusion  
 807 when exposed to ambient air whereas hypoxic episcleral vessels (embedded in  
 808 episcleral tissue) did not reoxygenate. Error bars represent the standard error of the  
 809 mean. The green fitted line is pulse oximeter data ( $\pm 2\%$   $\text{SO}_2$  uncertainty quoted by  
 810 the manufacturer not depicted for clarity).



811



813 **Table 3.** Calculated values of '1/2 time to reoxygenation' ( $T_{1/2}$ ) for 4 subjects,  
814 repeated twice per subject.

815

Subject	Data set	$T_{1/2}$ (seconds)
<b>A</b>	(i)	6.6
	(ii)	4.1
<b>B</b>	(i)	3.0
	(ii)	2.9
<b>C</b>	(i)	2.1
	(ii)	3.4
<b>D</b>	(i)	2.2
	(ii)	3.2
<b>Average</b>		<b>3.4</b>
<b>Standard Deviation</b>		<b>1.4</b>

816